An Innovative Design of a Permanent Magnet-Assisted Synchronous Reluctance Motor to Improve Torque Performance for High Speed Applications

Md Jabed Hossain, Paxton Schroeder, Josef Frankhouse, and Roy A McCann
Department of Electrical Engineering and Computer Science (EECS)
University of Arkansas
Fayetteville, AR, USA
mjhossai@uark.edu

2024 IEEE Energy Conversion Congress and Exposition (ECCE) | 979-8-3503-7606-7/24/$31.00 ©2024 IEEE | DOI: 10.1109/ECCE55643.2024.10861378

***Abstract*—This article introduces a novel design for the stator and rotor laminations of a three-phase permanent magnet-assisted synchronous reluctance motor (PMASynRM) to improve torque performance for high-speed applications. The design focuses on optimizing both reluctance torque and magnet alignment torque to achieve maximum torque output. The main innovation of this study is introducing a greater number of rectangular stator slots to increase power density and reduce torque ripples. Furthermore, the novel rotor lamination design incorporates a unique flux barrier to enhance the sinusoidal flux density at the airgap, thereby reducing the cogging torque. This project addresses the challenging task of manufacturing complex rotor and stator laminations through the application of metal additive manufacturing methods. To highlight the benefits of the proposed PMASynRM model, factors such as air gap flux density, output torque, back electromotive force (Back-EMF), saliency ratio, and efficiency are compared to those of a conventional IPM motor using finite element analysis (FEA). The results affirm that the novel PMASynRM demonstrates improved torque profiles, increased power density, and reduced harmonic components in Back-EMF compared to the conventional model.**

Keywords—Permanent magnet assisted synchronous reluctance motor (PMASynRM), finite element analysis (FEA), airgap, cogging torque, torque ripple, metal additive manufacturing.

I. INTRODUCTION

With growing concerns about sustainability and eco-friendly development, there is a demand for highly efficient and compact electromechanical conversion systems. Therefore, energy-efficient electrical machines are crucial in areas such as power generation from renewable sources, heavy propulsion systems, and electric vehicles (EVs). In these contexts, PMASynRMs are well-suited because they integrate the advantages of both synchronous reluctance motors (SynRMs) and permanent magnet synchronous motors (PMSMs). These advantages include high torque density, minimal torque ripple, flux-weakening control, and a wide operating speed range [1-3].

Despite the PMASynRM being one of the most efficient motors on the market, many researchers continue to work on enhancing its power density and torque profile. Current research on PMASynRM performance mainly focuses on areas like the design of permanent magnets, the analysis of magnetic circuits, and the development of flux barriers to improve torque profiles and power density [4, 5].

In [6-8], researchers introduced and examined an uneven arrangement of PM barriers across various salient rotor configurations. The study investigates finding the optimal placement of permanent magnets within the flux barriers to reduce torque ripple [9]. The flux barrier of rotor serves to prevent magnetic leakage and improve reluctance torque confirmed by [10]. The reluctance torque of a PMASynRM can be improved and torque ripple reduced by carefully designing the core flux barrier, considering both its quantity and structure [11]. Arc-shaped and U-shaped flux barriers are commonly used structures that enhance the performance of PMASynRM. In particular, the arc-shaped flux barrier is beneficial for achieving higher torque density [12, 13]. The magnet-axis-shift (MAS) phenomenon occurs when the alignment of the rotor's magnetic field axis deviates from the rotor's geometric axis, usually due to irregularities in the magnetic structure. This proposed configuration, which includes irregular shape of permanent magnets and an asymmetrical rotor core, is designed to leverage the MAS effect [14-16]. Introducing axial skew in the stator or rotor geometry can significantly decrease torque ripple, along with an increased number of phases [17]. Integer slot distributed windings are used in modular permanent magnet (PM) motors to analyze torque performance, which is then compared to the performance of motors with fractional slot concentrated windings [18].

Cogging torque has a major impact on torque ripple under all operating conditions. It can be diminished in modular PM motors by using multiple stator slots [19]. Altering the eccentricity of the magnetic pole decreases the harmonic content of the radial magnetic flux density in the air gap, thereby reducing cogging torque [20]. Jabed et al. utilized metal additive manufacturing technology to create complex stator and rotor laminations and examined different PM motors with higher number of stator slots [21-23].

This article presents a novel design for rotor and stator laminations intended to enhance the torque performance of PMASynRM. The paper evaluates the performance of this new model against that of a traditional IPM motor with identical

This work was supported in part by the U.S. National Science Foundation (NSF) within the Industry/University Cooperative Research Center (I/UCRC) on Grid-Connected Advanced Power Electronic Systems (GRAPES) through NSF GRAPES Phase III under Grant 1939144.

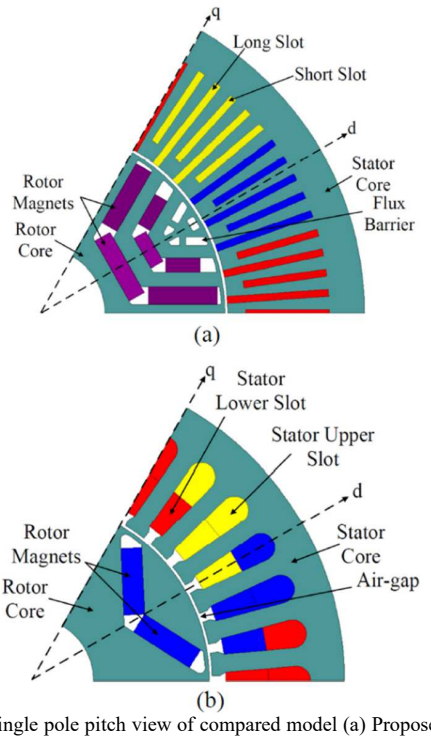

Fig. 1. Single pole pitch view of compared model (a) Proposed PMASynRM (b) Conventional IPM motor.

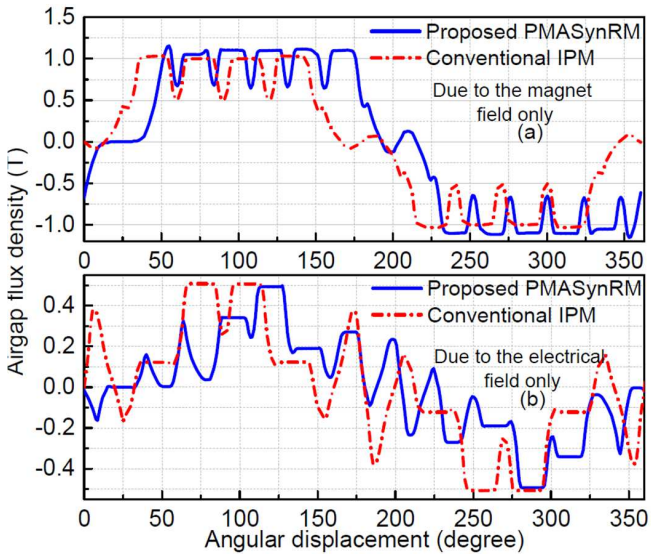

Fig. 2. Radial airgap flux density (a) Due to magnet field only (b) Due to electrical field only.

dimensions and electrical loading using FEA. The key contributions of this study are summarized as follows:

- Increasing the number of stator slots leads to higher torque density and reduced torque ripples.
- Implementing rectangular stator slots enhances the slot fill factor, allowing for the use of hairpin winding technology to increase power density.
- The innovative rotor structure design effectively reduces the radial flux density's eccentricity at the airgap, thereby decreasing cogging torque. Additionally, this rotor design ensures higher back-EMF with reduced harmonic content.

TABLE I
IMPORTANT SPECIFICATIONS OF ANALYSIS MODELS

Parameters	Unit	Conventional IPM	Proposed PMASynRM
Rated speed	r/min	1890	1890
Phase current	Arms	727.80	582.24
Stator outer diameter	mm	120	120
Stator bore diameter	mm	69.5	69.5
Outer diameter of rotor	mm	34.2	34.2
Stack length	mm	40.029	40.029
No. of poles/Slots		6/36	6/90
No. of turns in each slots		1	1
Magnet type		NdFeB	NdFeB
Soft iron rotor & stator core materials		M19_26G	M19_26G
Airgap length	mm	0.55	0.55
No. of phases		3	3

II. DESIGN OF PMASYNRM

A. Bacis Mathematical Expression of PMASynRM

The electromagnetic torque of a PMASynRM in steady-state operation is determined as follows,

$$T_e = \frac{3}{2} p \left(\left(L_d - L_q \right) i_d i_q + \lambda_{pm} i_q \right) \tag{1}$$

here, λ_{pm}, p, i_d, i_q, L_d, and L_q represents the flux linkage due to PM, the number of poles, the direct axis current, the quadrature axis current, the direct axis inductance, and the quadrature axis inductance, respectively.

The flux linkage of a PMASynRM along the d-axis and q-axis is obtained as follows,

$$\begin{cases} \lambda_d = \lambda_{pm} + L_d i_d \\ \lambda_q = L_q i_q \end{cases} \tag{2}$$

where, λ_d and λ_q denote the flux linkage along the d-axis and q-axis, respectively.

The cogging component of a PMASynRM, represented using Fourier series expansion, is expressed as follows,

$$T_{cog} = p \sum_{k=1}^{\infty} T_{pk} \, sin(N_s k\theta) \tag{3}$$

where N_s stands for the number of stator slots, θ denotes the rotor position, and T_{pk} stands for the Fourier coefficient of cogging torque per magnet.

The back-EMFs of a PMASynRM is obtained as follows,

$$E_{ph} = 4.44 \times f_s \times N_{etpph} \times k_w \times \varphi_p \tag{4}$$

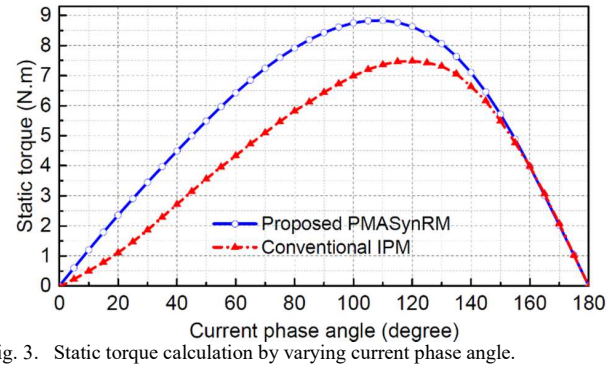

Fig. 3. Static torque calculation by varying current phase angle.

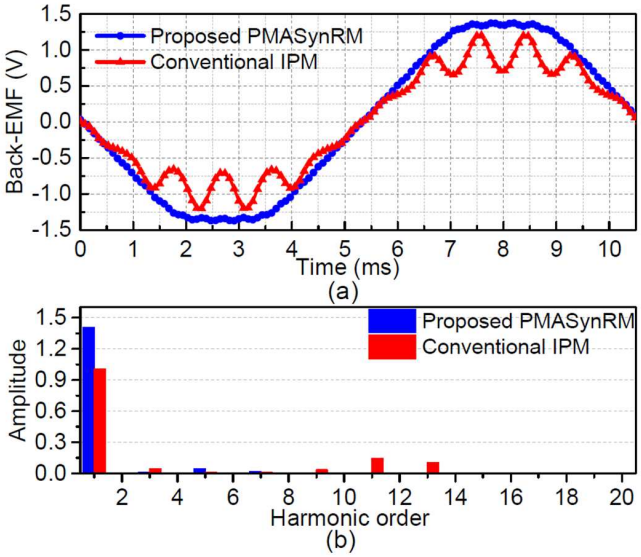

Fig. 4. Back EMFs characteristics (a) Back EMF for a phase A (b) Harmonics analysis.

where, N_{etpph} represents the number of effective turns per phase, f_s is the rated power supply frequency k_w is the winding factor, φ_p denotes the flux per pole.

The electrical loading of a PMASynRM was determined using the following equation:

$$L_{ele} = \frac{3 \times 2 \times N_t \times N_{cp} \times I_c}{\pi D} \quad (5)$$

where, I_c denotes the coil current, N_t is the number of turns in each coil, D stands for the bore diameter, and N_{cpph} represents the number of coils per phase.

The calculation of the number of coils per phase is as follows,

$$N_{cp} = \begin{cases} \frac{N_s}{2m}; for\ single-layer\ winding \\ \frac{N_s}{m}; for\ double-layer\ winding \end{cases} \quad (6)$$

here, m denotes the number of phases.

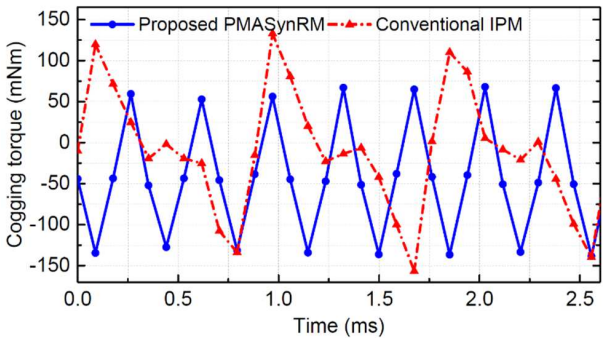

Fig. 5. Comparison of cogging torque of proposed model.

B. Proposed PMASynRM and Conventional IPM Model

A single pole of the proposed PMASynRM model is depicted in Fig. 1(a). The stator is equipped with three-phase distributed windings and 90 slots, designed for a six-pole machine. To increase the number of slots without compromising mechanical strength, two types of slots are utilized in the stator. The rotor has three levels of flux barriers but only two levels of permanent magnet arrangement, with all magnets being NdFeB magnets. In the illustration, the d-axis indicates the magnetic direction caused by the permanent magnets, while the q-axis is located 90 electrical degrees counterclockwise from the d-axis.

For design analysis, a conventional IPM motor with 36 slots and double-layer distributed windings, with the same dimensions as the proposed model, was selected. The rotor of this conventional motor includes V-shaped permanent magnets within the rotor core, featuring six poles as shown in Fig. 2(b). The dimensions, such as shaft diameter, stator outer diameter, stator bore diameter, rotor outer diameter, and air gap, are identical for both models. The key design specifications for both the proposed PMASynRM and conventional IPM motors are provided in Table I. Both models utilize M19_26G materials for their stator and rotor cores.

III. FEA Analysis and Result Discussion

A. Airgap Flux Density

The flux density at the air gap is crucial for determining the motor's torque output. Fig. 2(a) shows a comparison of the radial air gap flux density between the proposed PMASynRM and the conventional IPM motors under no-load conditions. The upper graph illustrates the radial air-gap flux density influenced solely by the magnetic field. The average flux density for the PMASynRM is calculated to be 0.77 T, compared to 0.64 T for the conventional IPM motor, although the volume of permanent magnets in the proposed model is slightly higher than in the conventional model. However, the increased power density in the proposed model outweighs the additional cost of the magnets used.

The bottom figure compares the air gap flux density for both models under an electrical loading of 40 kA/m only. The current density, calculated to be 4.69 A/mm² from electrical loading using (5). Fig 2(b) shows that the average flux density for the

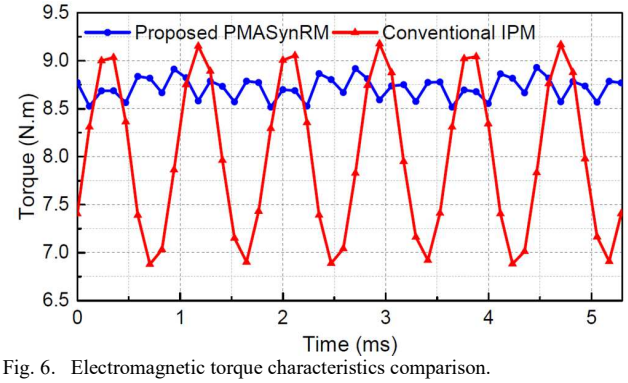

Fig. 6. Electromagnetic torque characteristics comparison.

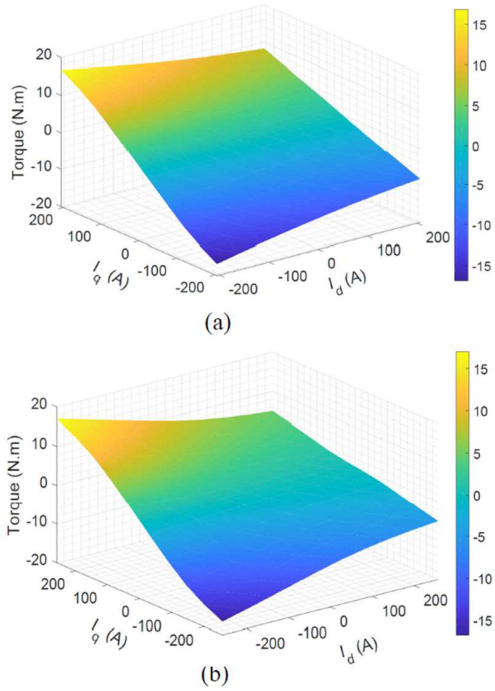

Fig. 7. Torque charateristics for different Id and Iq currents (a) Proposed PMASynRM (b) Conventional IPM.

proposed model is 0.19 T, while for the conventional model, it is 0.24 T. Despite this, the figure indicates that the conventional model exhibits more fluctuation, resulting in cogging torque.

B. MTPA Angle Calculation from Static Torque Grahp

The static torque characteristics curve of a PMASynRM demonstrates how torque output varies with the direction of current flow, which assists in devising effective control strategies. In this study, Maximum Torque per Ampere (MTPA) control strategy was adopted to pinpoint the best current phase angle for maximizing torque output. A systematic parametric sweep simulation was conducted by varying the phase angle of the phase current from 0 to 180 degrees in increments of 10 degrees. For the proposed model, the optimal MTPA angle was identified as 110 degrees, resulting in a torque of 8.83 N.m. Conversely, for the conventional model, the optimal MTPA angle was determined to be 120 degrees, achieving a torque of

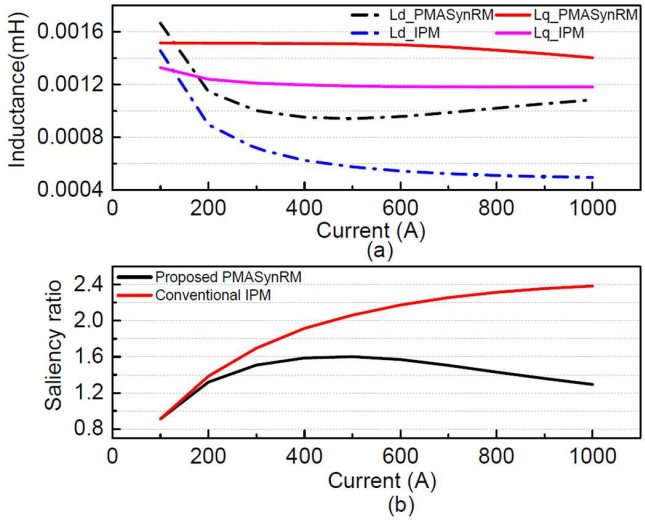

Fig. 8. Inductance profile (a) d-axis and q-axis inductances of compared model (b) comparison of saliency ratio.

7.48 N.m, as shown in Fig. 3.

C. No-load Back-EMFs Comparison for Single Phase

A greater air-gap flux density from the permanent magnet results in increased flux linkage, which subsequently causes a higher back-EMF magnitude in each phase. Under no load, higher back-EMF values indicate reduced losses and enhanced efficiency in the motor. Fig. 4 shows the comparison of the waveform and harmonic analysis of back EMF for both the proposed and conventional models. The RMS value of back-EMF in the novel model exceeds that of the conventional model by 37.21%, as depicted in Figure 4(a). It's important to mention that the conventional model exhibits a non-sinusoidal waveform, which contributes to the generation of cogging torque.

The harmonics graph is essential for assessing the quality of the generated EMF. According to the conventional model depicted in Figure 4(b), there is more harmonic content compared to the proposed model. Specifically, it is evident that significant 11th and 13th harmonics are present in the wave of the conventional model.

D. Comparison of Cogging Torque

Cogging torque in a permanent magnet motor primarily arises from the interaction between the permanent magnets and the stator teeth, resulting in the appearance of this unwanted torque. Additionally, variations in magnetic flux distribution and fluctuations in the distribution of back-EMFs can also contribute to cogging torque. Fig. 5 provides a comparison of cogging torque between the two models. The proposed model shows a lower peak-to-peak cogging torque value of 0.21 N.m, whereas the conventional model exhibits a higher value of 0.29 N.m. These differences in cogging torque can be attributed to the factors mentioned previously.

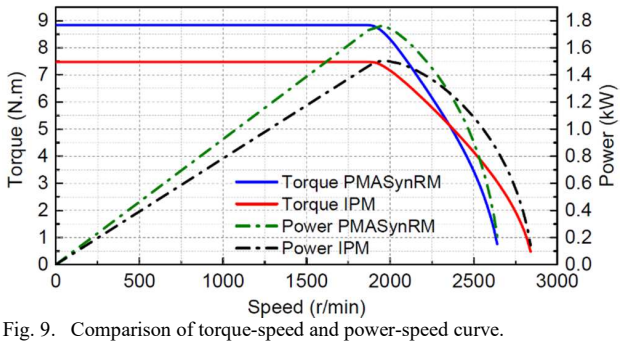

Fig. 9. Comparison of torque-speed and power-speed curve.

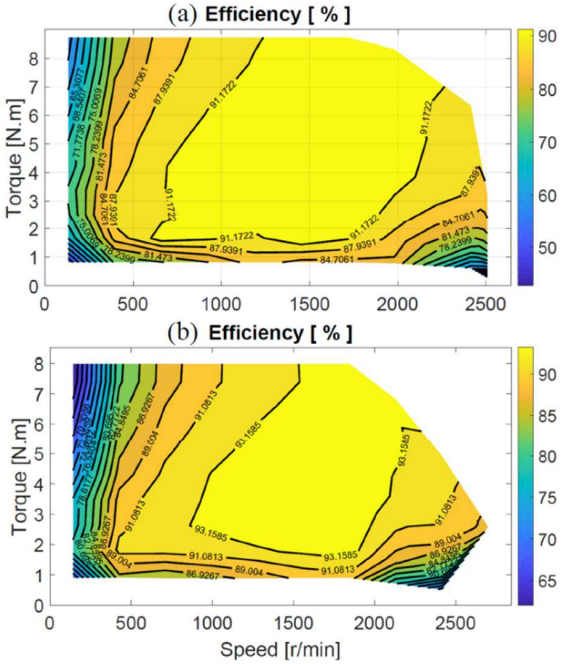

Fig. 10. Efficiency calculation at different speed condition (a) Proposed PMASynRM (b) Conventional IPM.

E. *Electromagnetic Torque Comparison*

The electromagnetic torque profiles of the proposed models in comparison to the conventional model under rated conditions, operating at a speed of 1890 rpm and an electrical loading of 40 kA/m is shown in Fig.6. The figure illustrates that the proposed model produces an electromagnetic torque of 8.72 N.m with a torque ripple of 4.75%. In contrast, the conventional model generates an average torque of 8 N.m but exhibits a significantly higher torque ripple of 28.73%, as detailed in Table II. The proposed model demonstrates superior torque characteristics due to its reduced torque ripple and higher torque density, resulting in smoother operation, minimized vibrations and noise, improved controllability, and an extended lifespan.

F. *Torque Calculation at Different Id and Iq Currents*

Fig. 7 displays a 3D graph that depicts torque variations with different combinations of d-axis and q-axis currents, providing valuable insights for designing control strategies and enhancing motor efficiency across various operating conditions.

Fig. 11. Prototyping of a PMASynRM

Specifically, Fig. 7(a) shows torque fluctuations for the proposed model, while Fig. 7(b) illustrates those for a conventional IPM motor. The graphs indicate that the proposed model exhibits a smoother surface, suggesting reduced torque ripple and implying more stable motor performance. Negative I_d current can optimize the magnetic flux in the salient pole machine, potentially increasing torque production as demonstrated in Fig. 7. Maximum torque is achieved with maximum negative I_d currents. It is evident that the conventional model requires a higher current loading to achieve the same level of output torque.

G. *Inductances and Saliency Ratio*

Fig. 8(a) and 8(b) show a comparison of the d and q-axis inductances as well as the saliency ratio between the proposed PMASynRM and the conventional IPM motors. The proposed model has higher d-axis and q-axis inductances than the conventional model at all operating currents. However, the saliency ratio of the PMASynRM is marginally less than that of the typical model across all operating current levels, with the difference being smaller at lower electrical loads and increasing at higher currents.

H. *Torque-Speed Curve Comparison*

The torque-power-speed characteristics of a permanent magnet motor play a critical role in assessing its maximum torque capacity and efficiency across different speeds. Fig. 9 reveals a comparison of the torque-power-speed curves for both models under investigation. The proposed PMASynRM motor exhibits higher torque within the constant torque region compared to the conventional IPM motor. Additionally, beyond the base speed of 1890 rpm, the torque and power of the conventional model decrease nearly to zero at higher speeds in comparison to the proposed model.

I. *Efficiency Comparison at Different Speed*

Copper loss accounts for the majority of total losses in both machines, with iron losses calculated using the Steinmetz empirical equation fitting to iron grade M19_26G, incorporating

TABLE II
COMPARISON OF PERFORMANCE OF THE ANALYSIS MODELS

Parameters	Unit	Conventional IPM	Proposed PMASynRM
Torque (average)	N.m	8.01	8.72
Torque ripple	%	28.73	4.75
Cogging torque (pk2pk)	N.m	0.291	0.213
Back EMFs (Phase A)	Vrms	0.723	0.992
Power (average)	kW	1.58	1.73
Power factor	%	99.68	99.48
Load angle	Degree	-33.86	-25.82
Copper loss	W	71.40	88.43
Core loss	W	13.50	17.66
Edddy current loss	W	0.130	0.527
Efficiency (average)	%	93.98	93.30

coefficients for eddy current and hysteresis losses. Table II provides a breakdown of these losses. Efficiency calculations include estimating friction losses in the bearings at 1% of total output power, in addition to iron loss (core loss and eddy current loss) and copper. Fig. 10 depicts a 3D plot showing efficiency in relation to torque and speed. Efficiency is lower at lower torque and speed levels for both models due to factors like core losses and winding resistance. The proposed PMASynRM motor achieves an average efficiency of 93.30%, while the conventional IPM motor achieves 93.98%. Despite the proposed model's high torque density, its higher copper losses contribute to this difference. This is mainly because the proposed model uses one conductor per slot, resulting in higher phase current for the same electrical loading and increased copper loss. This scenario represents a trade-off between efficiency and reducing parasitic capacitance in the stator winding.

IV. PROTOTYPING OF PMASYNRM

To verify the accuracy of both analytical and FEM results for the proposed design, the model was being physically constructed in the laboratory. As depicted in Fig. 11, the motor assembly includes a stator with 90 slots and a rotor with six poles. The stator, rotor, and hairpin stator winding were fabricated using metal additive technology. The thin wall thickness of the stator tooth makes it difficult for conventional methods like stamping, laser cutting, or water jet cutting to produce complex stator laminations with many slots. Metal additive manufacturing technology overcomes these challenges, enabling the production of complex stator and rotor laminations that were previously hard to manufacture. In this project, high carbon iron is used for the stator and rotor laminations, while copper is used for the hairpin winding.

The figure shows PLA-printed stator and rotor components, confirming the accuracy of their geometry. It also displays the printed stator and rotor laminations made of pure iron. Hairpin winding connections are employed in this project. Two distinct types of stator winding connections are designed along the stack length, with two connection ports at the top and bottom of the windings, as shown in Fig. 11. These ports are where the end winding connections are attached. Two end-winding connections are connected in parallel. Due to this parallel arrangement, the winding appears to have four layers, but it is actually a single layer with one winding per slot.

V. CONCLUSION

This article introduces a new design for the PMASynRM, aiming to enhance the contribution of permanent magnets to electromagnetic torque generation, reduce torque ripple, and achieve a higher no-load Back-EMF. The theoretical concept was applied in the proposed design, and results from 2-D FEM analysis showed an 8.86% increase in the total torque of the proposed PMASynRM compared to the conventional IPM motor model. This indicates improvements in torque and power density, along with a significant 83.47% reduction in torque ripple. The PM flux linkage increased notably due to precise sizing and positioning of the flux barrier and flux carrier. In the proposed model, the Back-EMF's rms value increased by approximately 37.21% compared to the conventional IPM motor, attributed to the effective design of rotor lamination. These findings suggest that the proposed machine is an optimal model for high-speed applications.

REFERENCES

[1] S. Ciceo, F. Chauvicourt, B. Varaticeanu, J. Gyselinck, and C. Martis, "PMASynRM late design-stage rotor shape NVH optimization," in 2020 International Conference on Electrical Machines (ICEM), 23-26 Aug. 2020 2020, vol. 1, pp. 278-283, doi: 10.1109/ICEM49940.2020.9270957.

[2] M. Z. Islam, A. Arafat, S. S. R. Bonthu, and S. Choi, "Design of a Robust Five-Phase Ferrite-Assisted Synchronous Reluctance Motor With Low Demagnetization and Mechanical Deformation," IEEE Transactions on Energy Conversion, vol. 34, no. 2, pp. 722-730, 2019, doi: 10.1109/TEC.2018.2882780.

[3] M. Xu, G. Liu, Q. Chen, J. Ji, and W. Zhao, "Design and Optimization of a Fault Tolerant Modular Permanent Magnet Assisted Synchronous Reluctance Motor With Torque Ripple Minimization," IEEE Transactions on Industrial Electronics, vol. 68, no. 9, pp. 8519-8530, 2021, doi: 10.1109/TIE.2020.3016263.

[4] Y. Kong, M. Lin, and G. Yang, "A Novel High Power Density Permanent Magnet Synchronous Machine with Wide Speed Range," in 2018 Asia-Pacific Magnetic Recording Conference (APMRC), 15-17 Nov. 2018 2018, pp. 1-1, doi: 10.1109/APMRC.2018.8601077.

[5] E. Trancho et al., "PM-Assisted Synchronous Reluctance Machine Flux Weakening Control for EV and HEV Applications," IEEE Transactions on Industrial Electronics, vol. 65, no. 4, pp. 2986-2995, 2018, doi: 10.1109/TIE.2017.2748047.

[6] J. Y. Alsawalhi and S. D. Sudhoff, "Design Optimization of Asymmetric Salient Permanent Magnet Synchronous Machines," IEEE Transactions on Energy Conversion, vol. 31, no. 4, pp. 1315-1324, 2016, doi: 10.1109/TEC.2016.2575138.

[7] W. Zhao, D. Chen, T. A. Lipo, and B. I. Kwon, "Performance Improvement of Ferrite-Assisted Synchronous Reluctance Machines Using Asymmetrical Rotor Configurations," IEEE Transactions on Magnetics, vol. 51, no. 11, pp. 1-4, 2015, doi: 10.1109/TMAG.2015.2436414.

[8] W. Zhao, T. A. Lipo, and B. I. Kwon, "Optimal Design of a Novel Asymmetrical Rotor Structure to Obtain Torque and Efficiency Improvement in Surface Inset PM Motors," IEEE Transactions on Magnetics, vol. 51, no. 3, pp. 1-4, 2015, doi: 10.1109/TMAG.2014.2362146.

[9] H. C. Liu, I. G. Kim, Y. J. Oh, J. Lee, and S. C. Go, "Design of Permanent Magnet-Assisted Synchronous Reluctance Motor for Maximized Back-EMF and Torque Ripple Reduction," IEEE Transactions on Magnetics, vol. 53, no. 6, pp. 1-4, 2017, doi: 10.1109/TMAG.2017.2663319.

[10] T. A. Huynh and M. F. Hsieh, "Comparative Study of PM-Assisted SynRM and IPMSM on Constant Power Speed Range for EV

Applications," IEEE Transactions on Magnetics, vol. 53, no. 11, pp. 1-6, 2017, doi: 10.1109/TMAG.2017.2707125.

[11] W. H. Kim et al., "Optimal PM Design of PMA-SynRM for Wide Constant-Power Operation and Torque Ripple Reduction," IEEE Transactions on Magnetics, vol. 45, no. 10, pp. 4660-4663, 2009, doi: 10.1109/TMAG.2009.2021847.

[12] T. A. Huynh and M. F. Hsieh, "Irreversible Demagnetization Analysis for Multilayer Magnets of Permanent Magnet-Assisted Synchronous Reluctance Machines Considering Current Phase Angle," IEEE Transactions on Magnetics, vol. 55, no. 7, pp. 1-9, 2019, doi: 10.1109/TMAG.2019.2911867.

[13] R. R. Moghaddam and F. Gyllensten, "Novel High-Performance SynRM Design Method: An Easy Approach for A Complicated Rotor Topology," IEEE Transactions on Industrial Electronics, vol. 61, no. 9, pp. 5058-5065, 2014, doi: 10.1109/TIE.2013.2271601.

[14] P. Winzer and M. Doppelbauer, "Comparison of synchronous machine designs with displaced reluctance axis considering losses and iron saturation," in 2015 IEEE International Electric Machines & Drives Conference (IEMDC), 10-13 May 2015 2015, pp. 1801-1807, doi: 10.1109/IEMDC.2015.7409308.

[15] Y. Xiao, Z. Q. Zhu, J. T. Chen, D. Wu, and L. M. Gong, "A Novel V-shape Interior Permanent Magnet Synchronous Machine with Asymmetric Spoke-type Flux Barrier," in 2020 International Conference on Electrical Machines (ICEM), 23-26 Aug. 2020 2020, vol. 1, pp. 382-388, doi: 10.1109/ICEM49940.2020.9270679.

[16] Y. Xiao, Z. Q. Zhu, J. T. Chen, D. Wu, and L. M. Gong, "A Novel Asymmetric Rotor Interior PM Machine with Hybrid-layer PMs," in 2020 IEEE Energy Conversion Congress and Exposition (ECCE), 11-15 Oct. 2020 2020, pp. 4029-4035, doi: 10.1109/ECCE44975.2020.9236015.

[17] R. Islam, I. Husain, A. Fardoun, and K. McLaughlin, "Permanent Magnet Synchronous Motor Magnet Designs with Skewing for Torque Ripple and Cogging Torque Reduction," in 2007 IEEE Industry Applications Annual Meeting, 23-27 Sept. 2007 2007, pp. 1552-1559, doi: 10.1109/07IAS.2007.240.

[18] Y. Li, Z. Q. Zhu, X. Wu, A. S. Thomas, and Z. Wu, "Comparative Study of Modular Dual 3-Phase Permanent Magnet Machines With Overlapping/Non-overlapping Windings," IEEE Transactions on Industry Applications, vol. 55, no. 4, pp. 3566-3576, 2019, doi: 10.1109/TIA.2019.2908138.

[19] G. J. Li, B. Ren, Z. Q. Zhu, Y. X. Li, and J. Ma, "Cogging Torque Mitigation of Modular Permanent Magnet Machines," IEEE Transactions on Magnetics, vol. 52, no. 1, pp. 1-10, 2016, doi: 10.1109/TMAG.2015.2477489.

[20] Y. Zhou, H. Li, G. Meng, S. Zhou, and Q. Cao, "Analytical Calculation of Magnetic Field and Cogging Torque in Surface-Mounted Permanent-Magnet Machines Accounting for Any Eccentric Rotor Shape," IEEE Transactions on Industrial Electronics, vol. 62, no. 6, pp. 3438-3447, 2015, doi: 10.1109/TIE.2014.2369458.

[21] M. J. Hossain, F. M. Felizco, M. T. Sandjong, and R. A. McCann, "A Novel Higher Stator Slots Surface-Mounted Permanent Magnet Motor for Variable Speed Drives," in 2023 IEEE Industry Applications Society Annual Meeting (IAS), 29 Oct.-2 Nov. 2023 2023, pp. 1-5, doi: 10.1109/IAS54024.2023.10406350.

[22] M. J. Hossain, K. Mackey, and R. A. McCann, "Enhancing Performance of Interior Permanent Magnet Motors Using Novel Stator Slot Designs," in 2023 North American Power Symposium (NAPS), 15-17 Oct. 2023 2023, pp. 1-6, doi: 10.1109/NAPS58826.2023.10318775.

[23] M. J. Hossain, P. Schroeder, and R. A. McCann, "Novel Design of Permanent Magnet-Assisted Synchronous Reluctance Motor Using Metal Additive Manufacturing Technology," in 2024 IEEE Green Technologies Conference (GreenTech), 3-5 April 2024 2024, pp. 80-84, doi: 10.1109/GreenTech58819.2024.10520449.